frontiers | Frontiers in Physics

TYPE Original Research
PUBLISHED 13 March 2023
DOI 10.3389/fphy.2023.1124026

OPEN ACCESS

EDITED BY
Huipeng Kang,
Innovation Academy for Precision Measurement Science and Technology (CAS), China

REVIEWED BY
Jinping Yao,
Shanghai Institute of Optics and Fine Mechanics (CAS), China
Xie Hong Qiang,
East China University of Technology, China

*CORRESPONDENCE
Zhiyang Lin,
suthing@hqu.edu.cn

SPECIALTY SECTION
This article was submitted to Atomic and Molecular Physics, a section of the journal Frontiers in Physics

RECEIVED 14 December 2022
ACCEPTED 28 February 2023
PUBLISHED 13 March 2023

CITATION
Chen Y, Man X, Liu B and Lin Z (2023), Nitrogen fluorescence emission pumped by femtosecond optical vortex beams. *Front. Phys.* 11:1124026. doi: 10.3389/fphy.2023.1124026

Nitrogen fluorescence emission pumped by femtosecond optical vortex beams

You Chen, Xiaoman Man, Binxian Liu and Zhiyang Lin*

Fujian Key Laboratory of Optical Beam Transmission and Transformation, College of Information Science and Engineering, Huaqiao University, Xiamen, China

An experimental investigation on nitrogen fluorescence emissions pumped by a single 800 nm fs optical vortex (OV) beam with different topological charges (TC) is reported. The intensity of the two prototype emission lines from neutral nitrogen molecules (N_2) and molecular nitrogen ions (N_2^+), *i.e.*, 337 nm and 391 nm, respectively, shows different TC dependences: the former slightly decreases as the TC increases, while the latter sharply decreases as the TC changes from zero to a non-zero value. The dependences of the 337-nm and 391-nm emission intensity on pulse energy are also different: the former shows a linear variation for different TCs, while the latter has an abrupt change in the slope when changing the TC. Furthermore, the dependence of the 337-nm emission intensity on gas pressure exhibits a plateau which is universal for different TCs. In contrast, the dependence of the 391-nm emission intensity on gas pressure shows an apparent hump which is respective of the TC. These actual new results will facilitate further theoretical study on the formation dynamics of the nitrogen fluorescence emissions induced by the OV beam, and inspire that such beam can been taken as a unique pure optical tool to manipulate the transitions between different electronic-vibrational states.

KEYWORDS

femtosecond, optical vortex beam, topological charge, nitrogen fluorescence emission, transition

Introduction

Since its discovery a few decades ago [1], femtosecond laser filamentation, which is formed by a dynamic competition between the self-focusing of the laser beam and the plasma defocusing caused by the ionization of air molecule or its major components (N_2 and O_2), has been continuously advancing our understanding of molecular ionization, dissociation, excitation and other dynamical processes through intriguing emissions such as fluorescence [2], lasing action [3–6], supercontinuum [7], and terahertz [8, 9]. Among them, the prototype nitrogen fluorescence emissions from the excited N_2 and N_2^+ molecules with a predominate line at 337 nm and 391 nm, respectively, can provide valuable clues to identify the formation mechanism of the molecular excited states for increasing the efficiency of population inversion, and thus the intensity of the remote cavity-free laser which holds great potential for the remote sensing and weather control [10–12].

The fluorescence emissions at 337 nm and 391 nm have been assigned to the transitions of N_2 $(C^3\Pi_u, \nu' = 0) \rightarrow N_2$ $(B^3\Pi_g, \nu = 0)$ and N_2^+ $(B^2\Sigma_g^+, \nu = 0) \rightarrow N_2^+$ $(X^2\Sigma_g^+, \nu' = 0)$, respectively. Two main types of experimental scenarios have been carried out to control the formation of $N_2(C^3\Pi_u)$ and N_2^+ $(B^2\Sigma_g^+)$. The first type is to adjust the intrinsic characteristic parameters of the laser such as pulse energy [2], wavelength [4] and

polarization [13], and even to employ a multiple-beam configuration for taking external pulses as seed [14–16], including the pump-probe technology. The pulse energy can directly influence molecular ionization rate, while the wavelength and polarization are related to the photon energy and spin angular momentum, respectively, which can influence photonic excitation and thus the transition selection rules. The second type is to control the macroscopic environment of the interaction region between nitrogen molecules or ions and laser by altering focusing condition [17, 18], pulse repetition [19], and gas pressures [17] or gas mixtures (*e.g.*, nitrogen-argon mixture and nitrogen-oxygen mixture) [20]. The fluorescence emissions at 337 nm and 391 nm can be generally observed and controlled in these scenarios, and from which alternative schemes have been derived for explaining the formation of the $N_2(C^3\Pi_u)$ and $N_2^+(B^2\Sigma_u^+)$. The former is attributed to three main possible schemes: collision-excitation [5, 13, 14, 21–23], collision-assisted intersystem crossing [13, 24, 25] and dissociative recombination through the reactions of $N_2^+ + N_2 \rightarrow N_4^+; N_4^+ + e \rightarrow N_2(C^3\Pi_u) + N_2$ [2, 26–28], while the latter is attributed to two main possible schemes: one is multi-photon ionization of the inner-valence electrons of N_2 [29]; the other is collision ionization of N_2 with a high energy electron [5, 13, 30]. Additionally, the second harmonic emission as well as supercontinuum emission can serve as a self-seeding pulse to start and enhance the lasing in N_2^+ molecules [17, 31]. However, a conclusive agreement on the formation mechanism of $N_2(C^3\Pi_u)$ or $N_2^+(B^2\Sigma_u^+)$ has not yet been reached, and thus further understanding and clarification of the mechanism behind the possible schemes requires, from an experimental point of view, alternative evidence by resorting to a unique technology.

Interestingly, the OV beam, possessing a spiral phase structure and thus exhibiting a unique ring-shaped transverse intensity profile, carries orbital angular momenta (OAM) which equals to a quantized TC [32] and can add a new degree of freedom to study strong-field physics [33, 34]. Indeed, it has been found that the intrinsic photon OAM can participate in the couple with the rotational and electronic motion, and makes the transitions forbidden by selection rules become possible when using the OV beam [35–38], while the bound electron can absorb the photon carrying an OAM [34, 37, 39–44]. On the other hand, the unique ring-shaped spatial distribution of the OV beam makes it can solely manipulate atoms or ions like a tweezer [45–47]. Therefore, the OV beam seems can not only affect the population of vibrational levels of electronic states, the transition probabilities and thus the emissions, but also affect the interaction between electrons, molecules and ions through the adjustable TC which is related to the size of the intensity ring, and accordingly, it offers a unique alternative to study nitrogen fluorescence emissions and to revisit the mechanism behind the aforementioned possible schemes. However, it still lacks direct experimental evidence on whether and how the OAM and ring-shape intensity profile are involved in the formation of $N_2(C^3\Pi_u)$ or $N_2^+(B^2\Sigma_u^+)$.

In this paper, using OV beams with different TCs, we systematically study the evolutions of the 337-nm and 391-nm emission intensity with pulse energy and gas pressure. Considering the advantages of the OV beam, a simultaneous control on the intrinsic process and the macroscopic region of the interaction between molecules and the laser is expected. It is found that the 391-nm emission sharply decreases as the TC increases while the 337-nm emission slightly depends on the TC. Moreover, the 337-nm emission exhibits a similar linear variation with the pulse energy for different TCs, while the evolution of the 391-nm emission with the pulse energy changes as the TC changes. For different TCs, the two emissions also exhibit different dependences on the gas pressure. These observations suggest that the OV beam is a unique and flexible toolkit to manipulate nitrogen fluorescence emissions.

Methods

In our experiments, femtosecond pulses generated by a commercial Ti:sapphire laser system (Astrella, Coherent, Inc.) are focused by an $f = 400$ mm convex lens into a gas chamber with a base pressure below 10^{-5} Pa, as shown in the left-hand panel of Figure 1. The pulse's central wavelength, duration and repetition of the pulse are 800 nm, 45 fs and 1 kHz, respectively. The variation of the pulse energy is achieved by a gradual neutral density filter (NDF) with a diameter of 50 mm. Spiral phase plates (SPP) with a high damage threshold are employed for generating femtosecond OV with different TCs of n. A beam splitter (BS) with a high splitting ratio of 99:1 is used to splitter the OV beam and steer the weak one into a CCD camera which can measure and monitor the spatial profile of the pulses. The measured transverse intensity profiles of the beams display rings with different radii, see the right-hand panels of Figure 1. The beam for n = 0 is a regular Gaussian beam. In special, the radius of the intensity ring increases as n increases, which is consistent with theoretical results showing the radius is proportional to $\sqrt{|n|}$ [48]. The uncertainty of the pulse energy is estimated to be less than 10%, which will not affect the comparison of data at different TCs and the consequent conclusion.

The chamber is filled with pure nitrogen gas at different pressures by a fine valve, and visible filaments with lengths of 10 mm–35 mm are formed. The fluorescence emissions produced from the chamber after the filament generation area are filtered by a combination of an 800 nm notch filer followed by a two-color filter (BG 40). The combination transmits the spectral components shorter than 400 nm but blocks the other accompanying emissions and attenuates largely the fundamental pulse as its intensity is too high.

The filtered pulses passing through a replaceable band-pass filter are coupled into a fiber spectrometer (Ocean Optics, HR4000) by means of an $f = 50$ mm fused silica lens followed by another $f = 100$ mm fused silica lens placed on a two-dimension moving stage. To circumvent the saturation of the spectrometer when the fluorescence intensity is too high, another neutral density filter is mounted at the entrance to the spectrometer. Depending on the fluorescence intensity, different laser shots are performed for each individual measurement to reduce the error and ensure a sufficiently high statistical accuracy. By choosing appropriate pulse energy range as well as the gas pressure range in our measurement, the supercontinuum is carefully controlled to emerge beyond a high pressure.

Results and Discussions

In this paper, we concentrate on the measurements of the two typical emissions at 337 nm and 391 nm. We first confirm that the length of filaments formed in nitrogen gas increases as the pulse

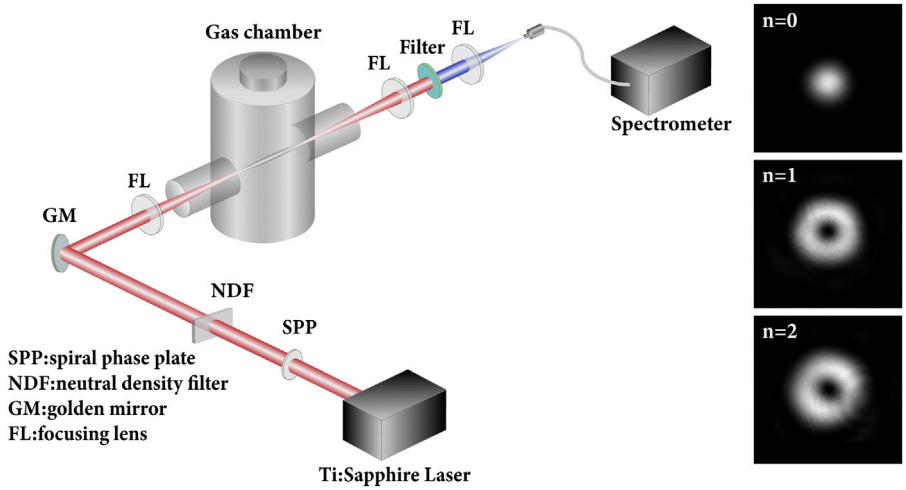

FIGURE 1
(Left panel) Schematic experimental setup. SSP: Spiral phase plate; NDF: neutral density filter; GM: golden mirror; FL: focusing lens; CCD: charged coupled device. (Right panel) Vortex beam profile measured by CCD when TCs are 0 (*i.e.*, Gaussian beam),1 and 2 with the same incident pulse energy.

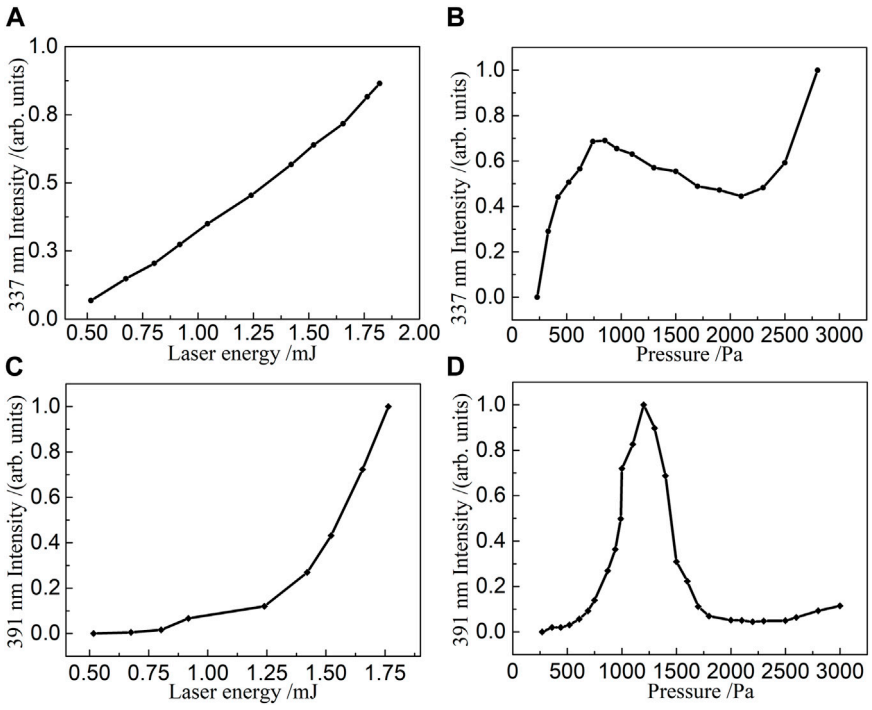

FIGURE 2
In the case of $n = 0$ **(A)** Intensity of the fluorescence emission at 337 nm as a function of the incident pulse energy with the nitrogen gas pressure of 1,200 Pa **(B)** Intensity of the fluorescence emission at 337 nm as a function of the nitrogen gas pressure with the pulse energy of 1.25 mJ. **(C,D)** is same as **(A,B)**, respectively, but for the lasting emission at 391 nm. For a better comparison, the maximum of each intensity curve is normalized to 1.

energy increases in the case of $n = 0$, *i.e.*, for a Gaussian beam. Then, according to the fact that the lasing signal is linear polarization and only propagates along the forward direction while the fluorescence signal is usually random polarization [4, 6], we have checked the polarizations of the forward emissions and found that the 391-nm emission for $n = 0$ is lasing signal while it is fluorescence signal for $n = 1$ or $n = 2$. Moreover, the measured 337-nm emissions for different TCs (*i.e.*, $n = 0$, one and 2) are all from the fluorescence signal. For $n = 0$, the 337-nm emission intensity, as shown in Figure 2A, increases nearly linearly with the increasing the pulse

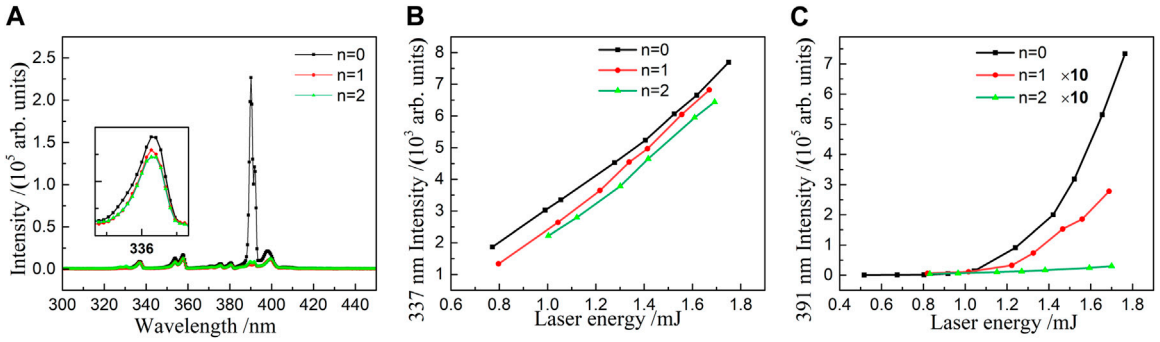

FIGURE 3
(A) Variation of the fluorescence spectra induced by filamentation of OV beams with different TCs in nitrogen gas when the pulse energy is 1.25 mJ and the gas pressure is 1,200 Pa. The enlarged fluorescence spectra at 337 nm are shown in the inset for visual convenience. **(B)** 337-nm emission intensity *versus* the pulse energy for different TCs when the nitrogen gas pressure is 1,200 Pa **(C)** 391-nm emission intensity *versus* the pulse energy for different TCs when the nitrogen gas pressure is 1,200 Pa, and the intensities for $n = 1$ and $n = 2$ are multiplied by a factor of 10.

energy, while the 391-nm lasing intensity first increases slowly with increasing the pulse energy, and then increases fast when the pulse energy is above 1.25 mJ, exhibiting an apparent knee point, see Figure 2C, which is consistent with the results presented in Ref. [17]. The significant increase of the 391-nm lasing intensity is due to that ionization rate increases exponentially with increasing the pulse energy which can directly affect the formation of $N_2^+(B^2\Sigma_u^+)$. For the 337-nm emission, the evolutions of the number of $N_2(C^3\Pi_u)$ and thus the fluorescence intensity with pulse energy proposed the aforementioned three possible schemes are similar [4]. Thus, the pulse energy is a simple but effective parameter which is used to influence the number of $N_2(C^3\Pi_u)$ or $N_2^+(B^2\Sigma_u^+)$.

Different features are also found from the evolutions of the 337-nm and 391-nm emission intensity with the gas pressure ranging from 250 Pa to 3,000 Pa at the pulse energy of 1.25 mJ, see Figures 2B, D. The 337-nm emission first increases fast until 900 Pa, and then decreases slowly and reaches its minimum at around 2,100 Pa, exhibiting an almost plateau-like tendency. Then, it increases fast again and exhibits a second increasing stage, as shown in Figure 2B. This stage can be attributed to the effective generation of supercontinuum which emerges at high pressures and takes over the 337-nm spectrum. In contrast, the 391-nm emission reaches its maximum at around 1,300 Pa, and then decreases significantly, leading to an obvious hump, as shown in Figure 2D, which is similar to the results presented in Ref. [17]. The significant decrease of the 391-nm lasing intensity beyond the pressure of 1,300 Pa is due to that the population inversion between the two involved states [*i.e.*, $N_2^+(B^2\Sigma_g^+, v = 0)$ and $N_2^+(X^2\Sigma_g^+, v' = 0)$] decreases at higher pressures, while the 428-nm lasing emission, which is from the transition of $N_2^+(B^2\Sigma_g^+, v = 0) \rightarrow N_2^+(X^2\Sigma_g^+, v' = 1)$, takes over as the generation of supercontinuum gradually approaches 428 nm with increasing pressure [17].

In order to control the excitation, ionization and collision occurring in the femtosecond filament which is related to the formation of $N_2(C^3\Pi_u)$ or $N_2^+(B^2\Sigma_u^+)$, we have repeated the same experiments using OV beams with different TCs. As mentioned above, the OV beam exhibits a ring-shaped intensity profile with a radius increasing with the TC, as depicted in right-hand panels of Figure 1. The OV beam is an effective tool to control the interaction region between the laser and nitrogen molecules, and influence the dynamics process. On the other hand, the OV beam carries an OAM scaled by the TC, which is related to the OAM-dependent absorption of light by a bound electron and may influence the transitions between different states, resulting in that the ionization process for the formation of $N_2^+(B^2\Sigma_u^+)$ can also be controllable. Thus, focusing on the role of the TC in the two protype transitions, we have extended the measurements to the OV beams with a higher TC, *i.e.*, $n = 1$ and $n = 2$.

Figure 3A displays the variation of spectra induced by the OV with the TC when the incident pulse energy is 1.25 mJ. It is obvious that the 337-nm emission intensity exhibits a weak dependence on the TC, see the inset in Figure 3A, while the 391-nm emission dominates in the case of $n = 0$ but decreases significantly for a higher TC. The former is further confirmed by the evolutions of the 337-nm emission intensity with the pulse energy for different TCs at the nitrogen gas pressure of 1,200 Pa, as shown in Figure 3B. As an overall view, the 337-nm emission intensity increases nearly linearly with increasing the pulse energy for different TCs and their slopes keep almost constant. In other words, the 337-nm emission intensity shows an identical change tendency for different TCs, exhibiting a less dependence on the TC which determines the spatial distribution of the pulse. As a result, the 337-nm emission intensity is influenced by the pulse energy, but it is irrespective of the spatial distribution.

In particular, the 337-nm emission intensity gradually decreases as the TC increases for a same pulse energy though the intensity gap is not large. This can be due to the ring-shaped energy distribution of the OV beam for a non-zero TC. The OV beam with a non-zero TC has an apparent hole in its center, which makes the peak intensity of the pulse decrease though the energy is the same as that in the case of $n = 0$, *i.e.*, for a Gaussian beam. The peak intensity influences the formation of $N_2(C^3\Pi_u)$ whose population becomes less as the peak intensity decreases, leading to a weak N_2 fluorescence emissions (337 nm, *etc.*) for a higher TC. On the other hand, in contrast to the 337-nm emission, the intensity of the N_2^+ fluorescence emissions (391 nm, *etc.*) which is directly related to the ionization process for the generation of $N_2^+(B^2\Sigma_u^+)$ shows a distinctly different dependence on the pulse energy: it increases significantly first, and then exhibits an apparent change of the slope when the pulse energy exceeds

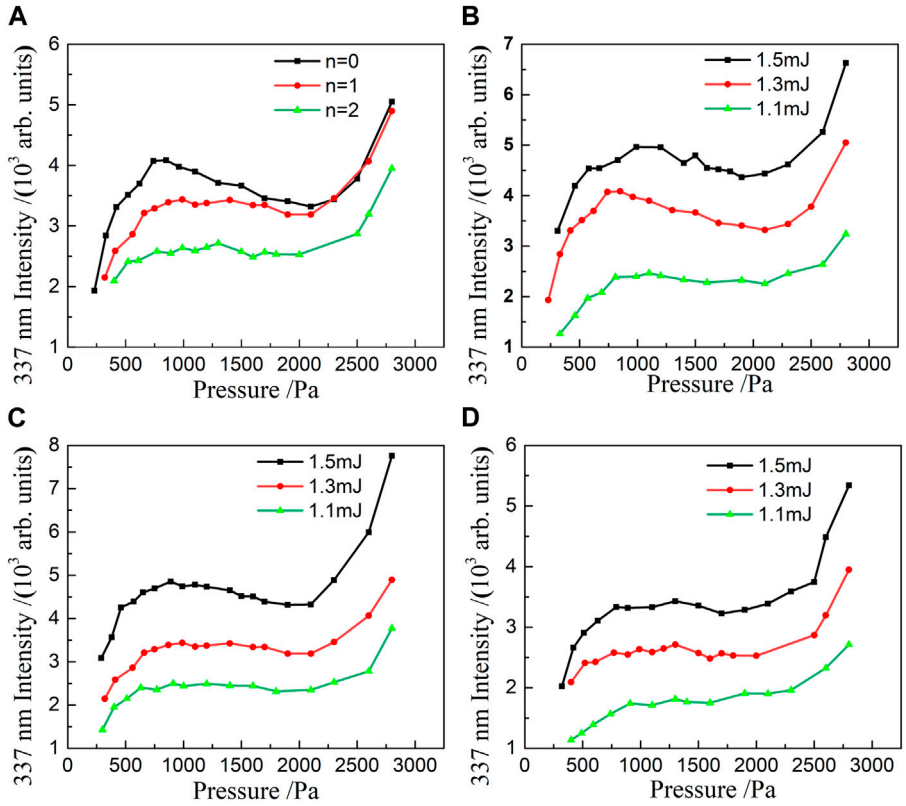

FIGURE 4
(A) Evolution of the fluorescence emission at 337 nm with nitrogen gas pressure for different TCs when the pulse energy is 1.25 mJ. **(B–D)** 337-nm emission intensity *versus* the gas pressure for three different pulse energies with the TC of 0,1 and 2, respectively.

1.25 mJ in the case of $n = 0$, see Figure 3C. Interestingly, for $n = 1$, the 391-nm emission intensity exponentially decreases, which is more than one order of magnitude lower than that of $n = 0$, while it becomes obscure when n increases up to two for the pulse energy range tested.

The 391-nm emission becomes weaker for a non-zero TC, indicating that the discrepancy between the Gaussian beam and OV beam will influence the intensity of the N_2^+ forward emissions, which can be understood from two aspects. First, the special spatial distributions of the OV beam makes the peak intensity of the pulse become weaker for a higher TC as the pulse energy is distributed along a bigger circle, resulting in a lower population of $N_2^+(B^2\Sigma_u^+)$. Because the ionization process for the generation of $N_2^+(B^2\Sigma_g^+)$ has a rate depending exponentially on the instantaneous electric field of the laser, the 391-nm emission will be greatly suppressed due to the decrease in the maximum electric field when the spatial distribution of the pulse changes from the Gaussian to the OV. As a result, the 391-nm emission intensity decreases with increasing the TC, exhibiting a tendency similar to that observed at 337 nm. Second, the interaction region between the OV beam and the molecules becomes larger as the TC increases, which should also influence the formation of $N_2^+(B^2\Sigma_u^+)$ and thus the 391-nm emission intensity. Furthermore, by qualitatively comparing the gap between the fluorescence intensity for $n = 1$ and $n = 2$ with that between the case of $n = 0$ and $n = 1$, we can find that the former is not obvious while the latter is large, see Figure 3C, which reveals that the exponential decrease of the ionization rate is mainly due to the decrease of the peak intensity of the laser, rather than the increase of the interaction region for a higher TC. It should be noted again that because the spiral phase profile of the OV field endows the photon with an OAM that equals to the TC, the OAM-dependent multi-photon absorption of a bound electron should be allowed by the transition selection rules, while the effect of photon OAM on photoionization is already trivial [49, 50], which will influence the plasma density and thus the intensity of the second harmonic [51]. The second harmonic can be taken as a seed to influence the lasing emission at 391 nm [17]. As we mentioned above, the 391-nm emission for $n = 0$ is lasing signal while that for $n = 1$ or $n = 2$ is fluorescence signal, which suggests that the lasing action at 391 nm is suppressed by the OV field, indicating that the TC can be taken as a novel additional parameter to control the transition responsible for the 391-nm emission and even the corresponding lasing action. As a whole, our experimental observations herein are the first-hand data for further theoretical study on nitrogen fluorescence emissions in the OV fields.

In order to provide more information for the benefit of exposing the characteristics of nitrogen fluorescence emissions, we plot the 337-nm emission intensity as a function of nitrogen gas pressure for different TCs with the pulse energy of 1.5 mJ in Figure 4. Since the evolution of the 337-nm emission intensity with the gas pressure in the case of $n = 0$ has been discussed above, we will focus on comparing the discrepancy of the evolutions between different

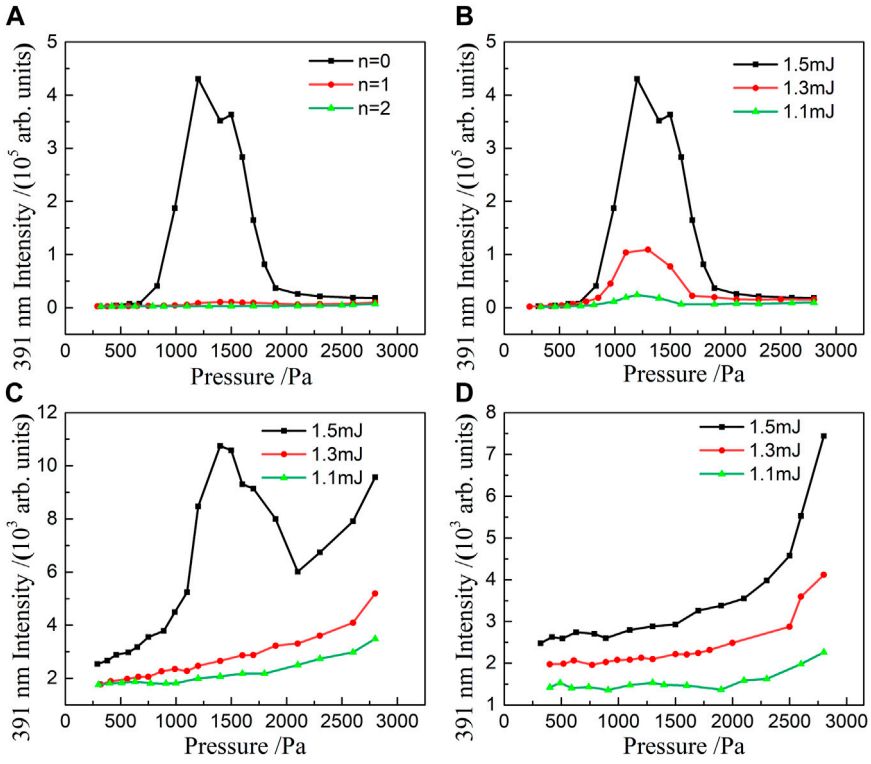

FIGURE 5
(A) Evolution of the emission at 391 nm with nitrogen gas pressure for different TCs when the pulse energy is 1.5 mJ. **(B–D)** 391-nm emission intensity *versus* the gas pressure for different pulse energies with the TC of 0,1 and 2, respectively.

TCs. As shown in Figure 4A, the evolutions of the 337-nm emission intensity with the pressure in both cases of $n = 1$ and $n = 2$ behave similarly to that of $n = 0$: it first increases fast and then decrease slowly, exhibiting an almost plateau-like tendency for a large pressure range, and then it increases fast again. This means that the change of the spatial distribution does not affect the evolution of the 337-nm emission. A similar but much smoother plateau-like tendency emerges for different energies in the cases of $n = 0$, $n = 1$ and $n = 2$, as shown in Figures 4B–D), respectively. Overall, the 337-nm emission intensity evolves similarly with the pressure for different TCs, and exhibits a plateau for a large pressure range. The plateau is irrespective of the TC and pulse energy, and seems to be universal. It should be noted that at the pressures above 2,400 Pa, the 337-nm emission intensity for $n = 0$ and $n = 1$ almost coincide and a similar second increasing state appears in all cases, which can be attributed to the effective generation of supercontinuum which dominates at high pressures and gradually suppresses the 337-mm emission.

In contrast to the 337-nm emission, the evolution of the 391-nm emission intensity with the gas pressure, as presented in Figure 5A, shows a clear TC dependence: an apparent hump emerges in the case of $n = 0$, while it disappears in the case of $n = 1$ or $n = 2$. Similar humps are also observed at other pulse energies for $n = 0$, as shown in Figure 5B. Figure 5A also shows that, compared to the case of $n = 0$, the 391-nm emission intensity for a non-zero TC exponentially decreases for the gas pressure range tested. It should be noted that, in our measurements, the supercontinuum emission is absent for most pulse energies or pressures, apart from for the pressures above 2,500 Pa at the highest pulse energy of 1.5 mJ for the case of n = 0. The latter covers a very small part which cannot influence the main trends of the curve for n = 0 in Figure 5 and thus the subsequent analysis. Furthermore, the results presented in Figures 5C, D show that the 391-nm emission intensity gradually increase as the gas pressure increases in the case of $n = 1$ or $n = 2$. In particular, the 391-nm emission intensity of $n = 1$, as shown in Figure 5C, exhibits an abrupt hump and a second increasing stage when the pulse energy is 1.5 mJ. The latter, similar to the 337-nm results presented above, can also be attributed to the influence of the supercontinuum which dominates at higher pressures. Overall, the 391-nm emission has a strong dependence on the TC, which suggests that the OV beam is a unique toolkit to control the transitions between different electronic-vibrational states and thus the fluorescence emissions.

Conclusion

In our study, employing OV beams with different TCs (*i.e.*, 0,1 and 2), the evolutions of the 337-nm and 391-nm emission intensity with pulse energy and gas pressure are experimentally investigated. It is found that the 337-nm emission intensity slightly decreases as the TC increases, while that at 391 nm sharply decreases as the TC changes from zero to a non-zero value. Meanwhile, the dependences of the 337-nm intensity on pulse energy show similar behaviors (*i.e.*, a linear variation) for different TCs, while the

dependences of the 391-nm intensity on pulse energy have an abrupt change in the slope when changing the TC. Furthermore, it is found that the dependence of the 337-nm emission intensity on gas pressure shows a universal plateau. In contrast, the dependence of the 391-nm emission intensity on gas pressure shows an apparent hump when the TC is zero, while it disappears for a non-zero TC, which is due to that the lasing action at 391 nm is suppressed by the OV field. These experimental findings are actual new which will inspire further theoretical investigations, and our study highlights that the versatile OV can be used as a unique tool to manipulate the transitions between different electronic-vibrational states and thus nitrogen fluorescence emissions.

Data availability statement

The original contributions presented in the study are included in the article/Supplementary material, further inquiries can be directed to the corresponding author.

Author contributions

YC: Measurements, pictures production, data analysis, preparation of the first draft. XM: Measurements, data analysis. BL: Data analysis. ZL: Conception and design of study, funding, interpretation of results, editing manuscript draft. All authors contributed to the article and approved the submitted version.

Funding

ZL acknowledges funding support by the National Natural Science Foundation of China (11504116) and the Scientific Research Startup Foundation of Huaqiao University (13BS406 and 605-50Y21003).

Acknowledgments

The authors of this paper acknowledge helpful discussions with Xudong Chen from Huaqiao University.

Conflict of interest

The authors declare that the research was conducted in the absence of any commercial or financial relationships that could be construed as a potential conflict of interest.

Publisher's note

References

1. Braun A, Korn G, Liu X, Du D, Squier J, Mourou G. Self-channeling of high-peak-power femtosecond laser pulses in air. *Opt Lett* (1995) 20(1):73–5. doi:10.1364/OL.20.000073

2. Xu HL, Azarm A, Bernhardt J, Kamali Y, Chin SL. The mechanism of nitrogen fluorescence inside a femtosecond laser filament in air. *Chem Phys* (2009) 360(1):171–5. doi:10.1016/j.chemphys.2009.05.001

3. Luo Q, Liu W, Chin SL. Lasing action in air induced by ultra-fast laser filamentation. *Appl Phys B* (2003) 76(3):337–40. doi:10.1007/s00340-003-1115-9

4. Yao J, Zeng B, Xu H, Li G, Chu W, Ni J, et al. High-brightness switchable multiwavelength remote laser in air. *Phys Rev A* (2011) 84(5):051802. doi:10.1103/PhysRevA.84.051802

5. Liu Y, Ding P, Lambert G, Houard A, Tikhonchuk V, Mysyrowicz A. Recollision-induced superradiance of ionized nitrogen molecules. *Phys Rev Lett* (2015) 115(13):133203. doi:10.1103/PhysRevLett.115.133203

6. Polynkin P, Cheng Y. *Air lasing*. Springer Cham: Springer (2018). p. 152.

7. Kasparian J, Rodriguez M, Méjean G, Yu J, Salmon E, Wille H, et al. White-light filaments for atmospheric analysis. *Science* (2003) 301(5629):61–4. doi:10.1126/science.1085020

8. Andreeva VA, Kosareva OG, Panov NA, Shipilo DE, Solyankin PM, Esaulkov MN, et al. Ultrabroad terahertz spectrum generation from an air-based filament plasma. *Phys Rev Lett* (2016) 116(6):063902. doi:10.1103/PhysRevLett.116.063902

9. Zhang Z, Chen Y, Cui S, He F, Chen M, Zhang Z, et al. Manipulation of polarizations for broadband terahertz waves emitted from laser plasma filaments. *Nat Photon* (2018) 12(9):554–9. doi:10.1038/s41566-018-0238-9

10. Rohwetter P, Kasparian J, Stelmaszczyk K, Hao Z, Henin S, Lascoux N, et al. Laser-induced water condensation in air. *Nat Photon* (2010) 4(7):451–6. doi:10.1038/nphoton.2010.115

11. Wolf JP. Short-pulse lasers for weather control. *Rep Prog Phys* (2018) 81(2):026001. doi:10.1088/1361-6633/aa8488

12. Xu HL, Chin SL. Femtosecond laser filamentation for atmospheric sensing. *Sensors* (2011) 11(1):32–53. doi:10.3390/s110100032

13. Mitryukovskiy S, Liu Y, Ding P, Houard A, Couairon A, Mysyrowicz A. Plasma luminescence from femtosecond filaments in air: Evidence for impact excitation with circularly polarized light pulses. *Phys Rev Lett* (2015) 114(6):063003. doi:10.1103/PhysRevLett.114.063003

14. Danylo R, Zhang X, Fan Z, Zhou D, Lu Q, Zhou B, et al. formation dynamics of excited neutral nitrogen molecules inside femtosecond laser filaments. *Phys Rev Lett* (2019) 123(24):243203. doi:10.1103/PhysRevLett.123.243203

15. Yao J, Li G, Jing C, Zeng B, Chu W, Ni J, et al. Remote creation of coherent emissions in air with two-color ultrafast laser pulses. *New J Phys* (2013) 15(2):023046. doi:10.1088/1367-2630/15/2/023046

16. Yao J, Jiang S, Chu W, Zeng B, Wu C, Lu R, et al. Population redistribution among multiple electronic states of molecular nitrogen ions in strong laser fields. *Phys Rev Lett* (2016) 116(14):143007. doi:10.1103/PhysRevLett.116.143007

17. Liu Y, Brelet Y, Point G, Houard A, Mysyrowicz A. Self-seeded lasing in ionized air pumped by 800 Nm femtosecond laser pulses. *Opt Express* (2013) 21(19):22791–8. doi:10.1364/OE.21.022791

18. Jing C, Zhang H, Chu W, Xie H, Ni J, Zeng B, et al. Generation of an air laser at extended distances by femtosecond laser filamentation with telescope Optics. *Opt Express* (2014) 22(3):3151–6. doi:10.1364/OE.22.003151

19. Zhang J, Hua L, Yu S, Wang Y, Zhu M, Xiao Z, et al. Laser-driven fluorescence emission in a nitrogen gas jet at 100 Mhz repetition rate. *Phys Rev A* (2021) 103(3):032822. doi:10.1103/PhysRevA.103.032822

20. Kartashov D, Ališauskas S, Andriukaitis G, Pugžlys A, Shneider M, Zheltikov A, et al. Free-space nitrogen gas laser driven by a femtosecond filament. *Phys Rev A* (2012) 86(3):033831. doi:10.1103/PhysRevA.86.033831

21. Kartashov D, Ališauskas S, Pugžlys A, Shneider MN, Baltuška A. Theory of a filament initiated nitrogen laser. *J Phys B: At Mol Opt Phys* (2015) 48(9):094016. doi:10.1088/0953-4075/48/9/094016

22. Ding P, Oliva E, Houard A, Mysyrowicz A, Liu Y. Lasing dynamics of neutral nitrogen molecules in femtosecond filaments. *Phys Rev A* (2016) 94(4):043824. doi:10.1103/PhysRevA.94.043824

23. Zheng W, Miao Z, Dai C, Wang Y, Liu Y, Gong Q, et al. formation mechanism of excited neutral nitrogen molecules pumped by intense femtosecond laser pulses. *J Phys Chem Lett* (2020) 11(18):7702–8. doi:10.1021/acs.jpclett.0c02337

24. Arnold BR, Roberson SD, Pellegrino PM. Excited state dynamics of nitrogen reactive intermediates at the threshold of laser induced filamentation. *Chem Phys* (2012) 405:9–15. doi:10.1016/j.chemphys.2012.05.019

25. Arnold CL, Akturk S, Mysyrowicz A, Jukna V, Couairon A, Itina T, et al. Nonlinear bessel vortex beams for applications. *J Phys B: At Mol Opt Phys* (2015) 48(9): 094006. doi:10.1088/0953-4075/48/9/094006

26. Talebpour A, Petit S, Chin SL. Re-focusing during the propagation of a focused femtosecond Ti:sapphire laser pulse in air. *Opt Commun* (1999) 171(4):285–90. doi:10.1016/S0030-4018(99)00498-8

27. Xu HL, Azarm A, Chin SL. Controlling fluorescence from N2 inside femtosecond laser filaments in air by two-color laser pulses. *Appl Phys Lett* (2011) 98(14):141111. doi:10.1063/1.3579246

28. Lin S, Zhang Y, Zhang H, Zhang Y, Chang M, Wang X, et al. Femtosecond laser-induced nitrogen fluorescence emission at different air pressures. *Phys Plasmas* (2021) 28(7):073302. doi:10.1063/5.0049248

29. Becker A, Bandrauk AD, Chin SL. S-matrix analysis of non-resonant multiphoton ionisation of inner-valence electrons of the nitrogen molecule. *Chem Phys Lett* (2001) 343(3):345–50. doi:10.1016/S0009-2614(01)00705-9

30. Liu Y, Ding P, Ibrakovic N, Bengtsson S, Chen S, Danylo R, et al. Unexpected sensitivity of nitrogen ions superradiant emission on pump laser wavelength and duration. *Phys Rev Lett* (2017) 119(20):203205. doi:10.1103/PhysRevLett.119.203205

31. Chu W, Li G, Xie H, Ni J, Yao J, Zeng B, et al. A self-induced white light seeding laser in a femtosecond laser filament. *Laser Phys Lett* (2014) 11(1):015301. doi:10.1088/1612-2011/11/1/015301

32. Allen L, Beijersbergen MW, Spreeuw RJC, Woerdman JP. Orbital angular momentum of light and the transformation of laguerre-Gaussian laser modes. *Phys Rev A* (1992) 45(11):8185–9. doi:10.1103/PhysRevA.45.8185

33. Shen Y, Wang X, Xie Z, Min C, Fu X, Liu Q, et al. Optical vortices 30 Years on: Oam manipulation from topological charge to multiple singularities. *Light: Sci Appl* (2019) 8(1):90. doi:10.1038/s41377-019-0194-2

34. De Ninno G, Wätzel J, Ribič PR, Allaria E, Coreno M, Danailov MB, et al. Photoelectric effect with a twist. *Nat Photon* (2020) 14(9):554–8. doi:10.1038/s41566-020-0669-y

35. Liu H, Li Y, You YS, Ghimire S, Heinz TF, Reis DA. High-harmonic generation from an atomically thin semiconductor. *Nat Phys* (2016) 13:262–5. doi:10.1038/nphys3946

36. Müller RA, Seipt D, Beerwerth R, Ornigotti M, Szameit A, Fritzsche S, et al. Photoionization of neutral atoms by *X* waves carrying orbital angular momentum. *Phys Rev A* (2016) 94(4):041402. doi:10.1103/PhysRevA.94.041402

37. Paufler W, Böning B, Fritzsche S. Strong-field ionization with twisted laser pulses. *Phys Rev A* (2018) 97(4):043418. doi:10.1103/PhysRevA.97.043418

38. Böning B, Paufler W, Fritzsche S. Above-threshold ionization by few-cycle bessel pulses carrying orbital angular momentum. *Phys Rev A* (2018) 98(2):023407. doi:10.1103/PhysRevA.98.023407

39. Zurch M, Kern C, Hansinger P, Dreischuh A, Spielmann C. Strong-field physics with singular light beams. *Nat Phys* (2012) 8(10):743–6. doi:10.1038/nphys2397

40. Mondal PK, Deb B, Majumder S. Angular momentum transfer in interaction of laguerre-Gaussian beams with atoms and molecules. *Phys Rev A* (2014) 89(6):063418. doi:10.1103/PhysRevA.89.063418

41. Scholz-Marggraf HM, Fritzsche S, Serbo VG, Afanasev A, Surzhykov A. Absorption of twisted light by hydrogenlike atoms. *Phys Rev A* (2014) 90(1):013425. doi:10.1103/PhysRevA.90.013425

42. Schmiegelow CT, Schulz J, Kaufmann H, Ruster T, Poschinger UG, Schmidt-Kaler F. Transfer of optical orbital angular momentum to a bound electron. *Nat Commun* (2016) 7:12998. doi:10.1038/ncomms12998

43. Kaneyasu T, Hikosaka Y, Fujimoto M, Konomi T, Katoh M, Iwayama H, et al. Limitations in photoionization of helium by an extreme ultraviolet optical vortex. *Phys Rev A* (2017) 95(2):023413. doi:10.1103/PhysRevA.95.023413

44. Afanasev A, Carlson CE, Schmiegelow CT, Schulz J, Schmidt-Kaler F, Solyanik M. Experimental verification of position-dependent angular-momentum selection rules for absorption of twisted light by a bound electron. *New J Phys* (2018) 20(2):023032. doi:10.1088/1367-2630/aaa63d

45. Jr GAS. The optical vortex coronagraph. *J Opt A Pure Appl Opt* (2009) 11(9): 094022–9. doi:10.1088/1464-4258/11/9/094022

46. Molina-Terriza G, Torres JP, Torner L. Twisted photons. *Nat Phys* (2007) 3(5): 305–10. doi:10.1038/nphys607

47. Grier DG. A revolution in optical manipulation. *Nature* (2003) 424(6950):810–6. doi:10.1038/nature01935

48. Géneaux R, Camper A, Auguste T, Gobert O, Caillat J, Taïeb R, et al. Synthesis and characterization of attosecond light vortices in the extreme ultraviolet. *Nat Commun* (2016) 7(1):12583. doi:10.1038/ncomms12583

49. Hartung A, Eckart S, Brennecke S, Rist J, Trabert D, Fehre K, et al. Magnetic fields alter strong-field ionization. *Nat Phys* (2019) 15(12):1222–6. doi:10.1038/s41567-019-0653-y

50. Fang Y, Guo Z, Ge P, Ma X, Han M, Yu X, et al. Strong-field photoionization of intense laser fields by controlling optical singularities. *Sci China Phys Mech Astron* (2021) 64(7):274211. doi:10.1007/s11433-021-1689-7

51. Li G, Ni J, Xie H, Zeng B, Yao J, Chu W, et al. Second harmonic generation in centrosymmetric gas with spatiotemporally focused intense femtosecond laser pulses. *Opt Lett* (2014) 39(4):961–4. doi:10.1364/OL.39.000961